IEEE Access
Multidisciplinary | Rapid Review | Open Access Journal

Received June 14, 2020, accepted June 28, 2020, date of publication July 1, 2020, date of current version July 20, 2020.

Digital Object Identifier 10.1109/ACCESS.2020.3006216

Fast 3D Beamforming Technique for Millimeter-Wave Cellular Systems With Uniform Planar Arrays

QASIM SULTAN, MOHAMMED SAQUIB KHAN, (Graduate Student Member, IEEE), AND YONG SOO CHO, (Senior Member, IEEE)

Department of Electrical and Electronics Engineering, Chung-Ang University, Seoul 06974, South Korea

Corresponding author: Yong Soo Cho (yscho@cau.ac.kr)

This work was supported by the National Research Foundation of Korea (NRF) grant funded by the Korean Government (MSIT) under Grant 2018R1A4A1023826 and Grant 2018R1A2B2002621.

ABSTRACT The beam search protocol in cellular systems requires a significant amount of search time and network resources in order to select a serving base station with the optimal beam pair. In 3D beamforming, the processing time increases significantly because the azimuth and elevation angles need to be considered during beam search. In this paper, we propose a fast 3D beamforming technique for millimeter wave (mmWave) cellular systems with a uniform planar array (UPA). In the proposed technique, the beam search time is reduced significantly by decomposing a UPA into a set of horizontal/vertical uniform linear arrays (ULAs), from which the optimal beam direction in azimuth/elevation angle is obtained. Two types of signals, Zadoff–Chu sequence and linear frequency modulated waveform are used for designing the beam search preamble (BSP), which allows a mobile user to distinguish beams in multi-cell multi-beam environments. The strengths and weaknesses of the two proposed BSPs are analyzed after performing simulation using a simple mmWave cellular system model with UPA. Furthermore, it is demonstrated that the proposed technique significantly reduces the beam search time, i.e., number of beam scans, as compared with the conventional technique.

INDEX TERMS Fast 3D beamforming, millimeter wave, uniform planar array, beam search preamble.

I. INTRODUCTION

There has been a rapid increase in the demand for high data rate transmission owing to the widespread use of smart devices and sensor nodes in various applications and services. Millimeter wave (mmWave) communication is a potential technology that enables the use of a wide bandwidth for highly advanced broadband cellular communication [1]–[3]. Highly directional beamforming antennas are necessary at both the base station (BS) and the mobile station (MS) to compensate for the high attenuation in the mmWave frequency band and extend the transmission range. With a small wavelength of an mmWave frequency, antenna arrays can be conveniently installed at the MS.

In recent years, there has been significant interest in 3D beamforming because of the 3D characteristics of real-world wireless channels [4], [5]. Compared to conventional 2D beamforming (which only involves the horizontal angle), 3D beamforming utilizes the elevation angle as well as the azimuth angle, thereby providing an additional degree of freedom. 3D beamforming can increase the signal-to-interference-plus-noise ratio (SINR) by adjusting the vertical antenna pattern in the direction of the MS, while reducing the interferences of adjacent sectors on the elevation angle. The major benefits of employing 3D beamforming include increased spectral efficiency, improved coverage, higher energy efficiency, high user capacity, less intercell and intersector interference, and improved cell edge user throughput. The ability to control the radiation pattern of an array in 3D beamforming is effective for controlling a multipath environment such that several signal components are constructively added at the location of the intended user. 3D beamforming is being considered for vehicular communication owing to the different sizes and shapes of surrounding infrastructure and for unmanned aerial vehicle (UAV) communication owing to the 3D characteristics of wireless

The associate editor coordinating the review of this manuscript and approving it for publication was Wen Chen.

channels [6]–[8]. Furthermore, 3D beamforming is also being considered for wireless connectivity in data centers using the 60 GHz band [9], [10].

Narrow-beam transmission and reception is effective for improving the link budget in mmWave frequencies. However, a misalignment between the transmitting (Tx) and receiving (Rx) beams may result in a significant loss in received power, particularly for systems with narrow beams. Therefore, beam alignment is necessary in mmWave communication systems to determine the optimal beam pair among all feasible beam pairs for maximizing beamforming efficiency [11]. Beam search is essential for the initialization stage and also in cases of radio link failure caused by blockages or an abrupt change of stations. The beam search operation in mmWave communication systems needs to be performed more frequently than in conventional communication systems because mmWave links are vulnerable to blocking and falling out of beam alignment. However, the beam search protocol in cellular systems requires a large amount of search time and network resources because it needs to select a serving BS with the optimal beam pair after examining the link qualities for all feasible beam pairs of the neighboring BSs. In 3D beamforming, the overhead for beam search operation is further increased because of the additional degrees of freedom [12]. Moreover, there is a significant increase in the overhead for beam search as the number of Tx and Rx beams increases [13].

In recent years, several techniques have been developed to efficiently employ 3D beamforming in various wireless communication networks. In [14], an interference coordination technique was investigated for cell-center and cell-edge users in 3D MIMO networks with different down tilts by dynamically adapting the shape of the vertical antenna pattern to the location of users. In [15], a location-based 3D beamforming technique was proposed for a high mobility UAV serving as a data relay by optimizing the beamforming direction of the UAV. In [16], a 3D beamforming algorithm that combined conventional horizontal and elevation beamforming for urban macro environments with different inter-site distances was proposed. The effect of user height on the coverage probability in mmWave cellular networks with 3D beamforming was investigated in [17]. An interference coordination algorithm was proposed for heterogeneous networks using 3D beamforming and statistical channel-state information from a macro-BS in [18]. A joint optimization algorithm of 3D beamforming and resource allocation for small cell backhaul in heterogeneous networks was proposed in [19]. The problem of using 3D beamforming in reconfigurable intelligent surface-assisted wireless communication networks was investigated in [20]. The radiation pattern at a BS equipped with a full dimensional antenna array was optimized to maximize the received signal-to-noise ratio (SNR) at the location of a target user. A new class of array structures and design techniques for 3D beamforming was presented in [21].

Many techniques have been proposed to reduce the overhead for beam search operation. In [22], two types of adaptive beam search protocols for fixed and adaptive modulation in mmWave communication systems were proposed. This proposed protocol employs an interactive beam search concept for fixed modulation and an iterative multi-level beam search concept for adaptive modulation. In [23], a fast beamforming algorithm was proposed for multi-group multi-cast beamforming design in large-scale wireless systems. A low-complexity high performance algorithm was proposed by leveraging the alternating direction method of multiplies together with convex-concave procedure. In this paper, a multicast beamforming algorithm was proposed assuming that channel state information is available at the transmitter. In [24], a fast transmit beamforming algorithm was proposed for distributed antenna systems using an iterative procedure and variable step sizes. In this approach, two or more distributed antennas work together to form a virtual array, which can align the transmitted signal phases at an intended user. A big challenge in distributed transmit beamforming systems is how to coordinate the sources (information sharing, timing synchronization, carrier synchronization) among distributed antennas. In [25], a fast initial access (beam alignment) procedure was proposed for mmWave 5G systems using the statistics of MS behavior. An online implementation method was proposed to acquire the MS statistics and adapt the initial access scanning procedure.

In this paper, we propose a fast 3D beamforming technique for mmWave cellular systems with a uniform planar array (UPA). In this technique, a UPA is decomposed into a set of horizontal/vertical uniform linear arrays (ULAs), from which the optimal beam direction in the azimuth/elevation domain is obtained. The optimal 3D beam direction is determined by combining the results obtained from each domain. The beam search time is further reduced by simultaneously transmitting beams in different directions from horizontal or vertical ULAs. Two types of signals Zadoff–Chu (ZC) sequence and linear frequency modulated (LFM) waveform are used for designing a beam search preamble (BSP), which allows MS to distinguish beams in multi-cell multi-beam environments. The properties of the proposed BSPs are analyzed in multi-cell multi-beam environments with carrier frequency offsets (CFOs). The CFO effect is particularly significant in cellular vehicle-to-everything (C-V2X) and UAV cellular communications.

The main contributions of this paper are:

- A fast 3D beamforming technique is proposed for mmWave cellular systems with a UPA, by decomposing a UPA into a set of horizontal/vertical ULAs and obtaining an optimal beam direction in the azimuth/elevation domain.
- Two BSPs (ZC-BSP and LFM-BSP) are proposed to reduce the beam search time further by simultaneously transmitting beams in different directions from horizontal/vertical ULAs and allowing an MS to distinguish beams in multi-cell multi-beam environments.
- The properties of the proposed BSPs are analyzed in multi-cell multi-beam environments with CFOs.

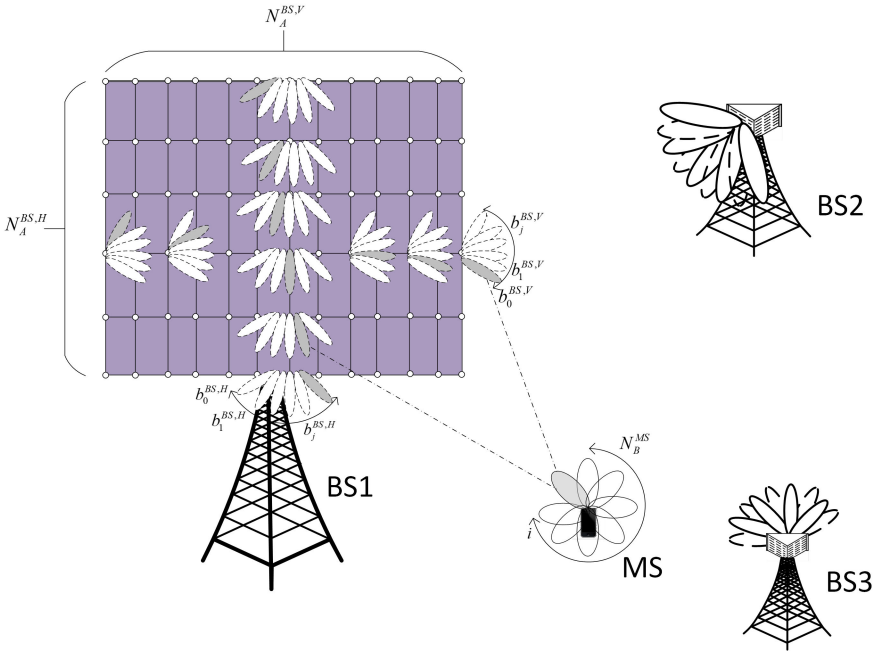

FIGURE 1. Proposed 3D beamforming technique for a mmWave cellular system with UPA.

Unlike [23], our proposed technique does not require channel state information because it is developed for beam search in the initialization stage. Also, unlike [24], the source coordination problem does not occur in the proposed technique because beams are transmitted from the same source (multiple ULAs in 3D beamformer). The beams transmitted from multiple ULAs at the BS are all synchronized in time and frequency. Unlike [25], the past statistics of MS behavior is not used in the proposed technique.

The remainder of this paper is organized as follows: In Section II, the concept of fast 3D beamforming technique for mmWave cellular systems with UPAs is described. In Section III, the preamble design technique for fast 3D beamforming using the ZC sequence is discussed. In Section IV, the use of the LFM waveform to design a beam search preamble for 3D beamforming is described. In Section V, an evaluation of the performance of the proposed techniques by computer simulation is presented. Finally, the conclusions of the study are listed in Section VI.

II. FAST 3D BEAMFORMING TECHNIQUE

For an mmWave cellular system with beamforming antennas, beam search is required for all feasible directions in the initialization stage because the position of the MS is not known to the BS. The processing time for beam search increases proportionally with product of the number of Tx beams and the number of Rx beams when the the exhaustive search technique is used [26], [27]. In 3D beamforming, the processing time is further increased because the elevation angle as well as the azimuth angle need to be considered in the beam search. When the exhaustive search technique is used for an mmWave system with a UPA, individual Tx beams are transmitted from BS until all the Tx beams in the azimuth angle are transmitted for a given elevation angle. The Rx beam sweeping is performed at MS to measure the SNR for each Tx–Rx beam pair. This process is repeated for all feasible elevation angles.

To reduce processing time, the UPA in the proposed technique is considered as a set of ULAs, as shown in Fig. 1. In Step 1, the UPA at the BS is decomposed into a set of horizontal ULAs. In this figure, $N_A^{BS,H}$ denotes the number of horizontal ULAs at the BS. The horizontal beam index (BID) $b_j^{BS,H}$, which represents the beam direction of the horizontal ULA, ranges from zero to $N_B^{BS,H} - 1$. Here, the subscripts, A and B, represent the antenna array and beam direction, respectively. In proposed technique, $N_B^{BS,H}$ horizontal beams are transmitted simultaneously from $N_A^{BS,H}$ horizontal ULAs at different azimuth angles. During this period, Rx beam sweeping is performed at the MS. The MS calculates the correlation values between the received signals and the reference signal and determines the Tx horizontal BID and the Rx BID that yield the highest correlation value. If $N_A^{BS,H}$ is smaller than $N_B^{BS,H}$ and given by $N_B^{BS,H} = s^H \times N_A^{BS,H}$ (s^H: integer), this process is repeated s^H times by changing the horizontal beams until all these beams are transmitted. If the UPA has $N_B^{BS,H}$ horizontal antenna arrays, then only one round of the Rx beam sweeping is required. In Step 2, the UPA at the BS is viewed as a collection of vertical ULAs. Here, $N_A^{BS,V}$ denotes the number of vertical ULAs. The vertical BID $b_j^{BS,V}$, which represents the beam direction of the vertical ULA, ranges from zero to $N_B^{BS,V} - 1$.

$N_B^{BS,V}$ vertical beams are simultaneously transmitted from $N_A^{BS,V}$ vertical ULAs at different elevation angles. During this period, Rx beam sweeping is performed at the MS. The MS determines the Tx vertical BID and the Rx BID that yields the highest correlation value. If $N_A^{BS,V}$ is smaller than $N_B^{BS,V}$ and given by $N_B^{BS,V} = s^V \times N_A^{BS,V}$ (s^V: integer), this process is repeated s^V times by changing vertical beams until all these beams are transmitted. In Step 3, a 3D beam is formed in the direction of the MS using the results of horizontal BID and vertical BID obtained from Steps 1 and 2. Thus, the number of beam scans required for the proposed 3D beamforming technique is given as $2 \times s^V \times s^H \times N_B^{MS}$. If the UPA has $N_B^{BS,H}$ horizontal antenna arrays and $N_B^{BS,V}$ vertical antenna arrays, only two rounds of Rx beam sweep are required. In this case, in the proposed technique, the processing time for beam search is only proportional to the number of Rx beams and not to the number of 3D Tx beams. Here, it is assumed that the distance between the BS and MS is considerably large, compared with the antenna size of the UPA at the BS. In this case, the spacing between the ULAs at the BS can be neglected, that is, the horizontal/vertical ULAs transmitting beams at different azimuth/elevation angles are assumed to have identical elevation/azimuth angles. It is also assumed that analog beamforming is used at both the BS and the MS during the beam search period. To measure the SNR for each Tx–Rx beam pair, the MS should be able to identify the Tx BID and the corresponding cell ID (CID) from the preambles received from the serving and neighboring BSs. For the proposed technique, as multiple preambles are received simultaneously from the serving and neighboring BSs, the preamble should be designed such that the inter-beam interference and inter-cell interference are minimal. In Section II and Section III, we propose two types of preambles that enable the MS to distinguish beams in multi-cell and multi-beam environments.

III. ZC-BASED 3D BEAMFORMING TECHNIQUE

The ZC sequence is widely used for designing synchronization signals, reference signals, and random-access preambles in LTE or 5G NR systems, owing to its good correlation property and low peak-to-average ratio (PAPR) [28]–[30]. To enable an MS to identify the Tx BID and the CID from the received signals, the BID needs to be designed in conjunction with the CID in the BSP. As multiple beams are transmitted in parallel in the proposed fast 3D beamforming technique, the horizontal BID $b_j^{BS,H}$ and $b_j^{BS,V}$ are distinguished by the amount of cyclic shift spacing in the proposed ZC-based BSP (ZC-BSP). In addition, the CID designed in conjunction with the horizontal/vertical BID in a ZC-BSP is distinguished by the root index of ZC sequence. In the proposed ZC-BSP, the BID and CID are mapped to the prime-length ZC sequence as follows:

$$x_{ZC}^{c,b}(n) = e^{\frac{j\pi r^c (n+Qb_j)(n+Qb_j+1)}{N_z}} \quad (1)$$

where $1 < r^c < N_z$ and $\gcd(r, N_z) = 1$. Here, N_z, r^c, and Q denote the length of the ZC sequence, root index for the CID c and cyclic shift spacing constant, respectively. As the horizontal and vertical beams are transmitted at different time slots, the BID b_j is used for notational convenience rather than the horizontal BID $b_j^{BS,H}$ and vertical BID $b_j^{BS,V}$. The ZC sequence has the property of constant envelop and zero autocorrelation. The cross-correlation between ZC sequences with different root indexes is $1/\sqrt{N_z}$. The number of available CIDs in the ZC-BSP is given by $N_z - 1$. To determine the performance of BID and CID detection, we analyze the correlation property of ZC-BSP in a multi-cell and multi-beam environment, as in (2), as shown at the bottom of the next page.

In (2), $y_i(n)$ is received signal on *ith* beam of a MS. Here, g_{TX}^{c,b_j}, $g_{RX,i}$, and h_i^{c,b_j} denote the transmit beamforming gain of the $b_j th$ beam of the BS with CID c, receive beamforming gain of the *ith* beam of the MS, and channel between the BS in the *cth* cell with $b_j th$ beam and *ith* beam of the MS, respectively. The channel is assumed to be a line-of-sight (LOS)-dominated flat fading channel. N_B^{BS} denotes the number of horizontal beam directions $N_B^{BS,H}$ in Step 1 and vertical beam directions $N_B^{BS,V}$ in Step 2. Here, $\bar{c}$ and $\bar{b}$ denote the reference CID and reference BID, respectively. Moreover, $\delta_i^{(c,b_j)}$ and $\varepsilon_i^{(c,b_j)}$ denote the symbol timing offset (STO) and CFO between the $b_j th$ Tx beam of the BS and *ith* Rx beam of the MS in the *cth* cell, respectively. As the distance between the BS and MS is assumed to be considerably large compared to the antenna spacing between ULAs at the BS, the STO and CFO can be approximated as δ_i^c and ε_i^c (i.e. not a function of the Tx beam or the Tx antenna array), respectively. Moreover, as the ULAs are transmitting beams in different directions from antenna arrays in the UPA at the same BS, the STOs between the ULAs and MS would be almost identical. The simplified notations (δ_i^c, ε_i^c) are used in the following discussions.

In (2), Γ_{ZC} represents the autocorrelation when the received beam is matched with the reference beam in the same cell. The terms inside the summation in Γ_{ZC} can be expressed as in (3), as shown at the bottom of the next page.

At the MS, correlation is performed by shifting the locally generated reference sequence. As is evident from (3), the correlation decreases in a *sinc−like* pattern as the CFO increases. The maximum peak occurs when the CFO is zero and the shift index (m) matches with the STO value δ_i^c. In this case, the autocorrelation value becomes one. In addition, the value of Γ_{ZC} in (2) would be high because the beamforming gain and channel gain are high. The beamforming and channel gains are generally high when the Tx and Rx beams are aligned. The STO can be estimated by performing the correlation operation for different values of m.

In (2), Ω_{ZC} represents the inter-beam interference when the received beam has a CID equal to that in the reference preamble ($c = \bar{c}$) and a different BID $\left(b_j \neq \bar{b}\right)$. The terms inside the summation in Ω_{ZC} can be rewritten

as (4), which is shown at the bottom of the page. Here,

$$\xi^{(\bar{c},Q,b,\bar{b},\delta,\varepsilon_i^{(\bar{c},b)})} = r^{\bar{c}}\left[Qb_j - Q\bar{b} - \delta_i^{\bar{c}} + m\right] - \varepsilon_i^{\bar{c}}. \quad (5)$$

In addition, μ is arbitrary integer. The correlation value in (4) would be high when the following condition is satisfied.

$$r^{\bar{c}}\left[Qb_j - Q\bar{b} - \delta_i^{\bar{c}} + m\right] - \varepsilon_i^{\bar{c}} = \mu N_z \quad (6)$$

In this case, the correlation peak may occur at incorrect positions, resulting in detection errors. To prevent the ambiguity condition, the cyclic shift spacing constant Q should be set such that it does not take the following values:

$$Q = \frac{\mu N_z + r^{\bar{c}}\delta_i^{\bar{c}} - r^{\bar{c}}m + \varepsilon_i^{\bar{c}}}{r^{\bar{c}}\Delta b}, \quad Q > 0 \quad (7)$$

$$\begin{aligned} r_{ZC,i}^{c,b_j}(m) &= \sum_{k=0}^{N_z-1} y_i(n)\left(x^{\bar{c},\bar{b}}(n-m)\right)^* \\ &= \sum_{c=0}^{N_c-1}\sum_{b_j=0}^{N_B^{BS}-1}\sum_{n=0}^{N_Z-1} g_{TX}^{c,b_j} g_{RX,i} h_i^{c,b_j} x_{ZC}^{c,b_j}(n-\delta_i^{(c,b_j)}) e^{\frac{j2\pi k\varepsilon_i^{(c,b_j)}}{N_z}}\left(x_{ZC}^{\bar{c},\bar{b}}(n-m)\right)^* \\ &= \Gamma_{ZC} + \Omega_{ZC} + \Upsilon_{ZC} + \Psi_{ZC} \end{aligned} \quad (2)$$

where

$$\begin{aligned} \Gamma_{ZC}(m) &= g_{TX}^{\bar{c},\bar{b}} g_{RX,i} \sum_{n=0}^{N_Z-1} h_i^{\bar{c},\bar{b}} x_{ZC}^{\bar{c},\bar{b}}(n-\delta_i^{(\bar{c},\bar{b})}) e^{\frac{j2\pi n\varepsilon_i^{(\bar{c},\bar{b})}}{N_z}}\left(x_{ZC}^{\bar{c},\bar{b}}(n-m)\right)^* \\ \Omega_{ZC}(m) &= \sum_{b_j=0,b_j\neq\bar{b}}^{N_B^{BS}-1} g_{TX}^{\bar{c},b_j} g_{RX,i} \sum_{n=0}^{N_Z-1} h_i^{\bar{c},b_j} x_{ZC}^{\bar{c},b_j}(n-\delta_i^{(\bar{c},b_j)}) e^{\frac{j2\pi n\varepsilon_i^{(\bar{c},b_j)}}{N_z}}\left(x_{ZC}^{\bar{c},\bar{b}}(n-m)\right)^* \\ \Upsilon_{ZC}(m) &= \sum_{c=0,c\neq\bar{c}}^{N_c-1}\sum_{b_j=0}^{N_B^{BS}-1} g_{TX}^{c,b_j} g_{RX,i} \sum_{n=0}^{N_Z-1} h_i^{c,b_j} x_{ZC}^{c,b_j}(n-\delta_i^{(c,b_j)}) e^{\frac{j2\pi n\varepsilon_i^{(c,b_j)}}{N_z}}\left(x_{ZC}^{\bar{c},\bar{b}}(n-m)\right)^* \\ \Psi_{ZC}(m) &= g_{RX,i}\sum_{n=0}^{N_Z-1} w_i(n)\left(x_{ZC}^{\bar{c},\bar{b}}(n-m)\right)^* \end{aligned}$$

$$\begin{aligned} &\sum_{n=0}^{N_Z-1} x_{ZC}^{\bar{c},\bar{b}}(n-\delta_i^{\bar{c}}) e^{\frac{j2\pi n\varepsilon_i^{\bar{c}}}{N_z}}\left(x_{ZC}^{\bar{c},\bar{b}}(n-m)\right)^* \\ &= \sum_{n=0}^{N_z-1} e^{\frac{j\pi r^{\bar{c}}\left(n-\delta_i^{\bar{c}}+Q\bar{b}\right)\left(n-\delta_i^{\bar{c}}+Q\bar{b}+1\right)}{N_z}} e^{\frac{j2\pi n\varepsilon_i^{\bar{c}}}{N_z}}\left(e^{\frac{j\pi r^{\bar{c}}\left(n-m+Q\bar{b}\right)\left(n-m+Q\bar{b}+1\right)}{N_z}}\right)^* \\ &= e^{\frac{j\pi r^{\bar{c}}}{N_z}\left[\left(\delta_i^{\bar{c}}\right)^2 - 2Q\bar{b}\delta_i^{\bar{c}} - \delta_i^{\bar{c}} - m^2 + 2Q\bar{b}m + m\right]} \cdot e^{j\pi\left(\varepsilon_i^{\bar{c}} - 2\delta_i^{\bar{c}} + 2m\right)(N_z-1)/Nz} \cdot \frac{\sin\pi\left(\varepsilon_i^{\bar{c}} - 2\delta_i^{\bar{c}} + 2m\right)}{\sin\left(\pi\left(\varepsilon_i^{\bar{c}} - 2\delta_i^{\bar{c}} + 2m\right)/N_z\right)} \end{aligned} \quad (3)$$

$$\begin{aligned} &\sum_{b_j=0,b_j\neq\bar{b}}^{N_B^{BS}-1}\sum_{n=0}^{N_Z-1} x_{ZC}^{\bar{c},b_j}(n-\delta_i^{\bar{c}}) e^{\frac{j2\pi n\varepsilon_i^{\bar{c}}}{N_z}}\left(x_{ZC}^{\bar{c},\bar{b}}(n-m)\right)^* \\ &= \sum_{n=0}^{N_z-1} e^{\frac{j\pi r^{\bar{c}}\left(n-\delta_i^{\bar{c}}+Qb_j\right)\left(n-\delta_i^{\bar{c}}+Qb_j+1\right)}{N_z}} e^{\frac{j2\pi n\varepsilon_i^{\bar{c}}}{N_z}}\left(e^{\frac{j\pi r^{\bar{c}}\left(n-m+Q\bar{b}\right)\left(n-m+Q\bar{b}+1\right)}{N_z}}\right)^* \\ &= \underbrace{e^{\frac{j\pi r^{\bar{c}}}{N_z}[Qb_j(Qb_j+1)]}}_{x^{\bar{c},b_j}(0)} \cdot \underbrace{e^{\frac{j\pi r^{\bar{c}}}{N_z}[Q\bar{b}(Q\bar{b}+1)]}}_{x^{\bar{c},\bar{b}}(0)^*} e^{\frac{j2\pi r^{\bar{c}}}{N_z}\left[\left(\delta_i^{\bar{c}}\right)^2 - 2Qb_j\delta_i^{\bar{c}} - \delta_i^{\bar{c}} - m^2 + 2Q\bar{b}m + m\right]} \sum_{n=0}^{N_z-1} e^{\frac{j2\pi}{N_z}n\left[r^{\bar{c}}(Qb_j - Q\bar{b} - \delta_i^{\bar{c}} + m) - \varepsilon_i^{\bar{c}}\right]} \\ &= \begin{cases} x^{\bar{c},b_j}(0)x^{\bar{c},\bar{b}}(0)\cdot N_z & if\ \xi^{(\bar{c},Q,b_j,\bar{b},\delta_i^{\bar{c}},m,\varepsilon_i^{\bar{c}})} = \mu N_z \\ 0 & otherwise \end{cases} \end{aligned} \quad (4)$$

where $\Delta b = b_j - \bar{b}$. The maximum value of Q can be found as

$$Q_{\max} = \left\lfloor \frac{N_z}{N_B^{BS}} \right\rfloor. \tag{8}$$

The summation term in Ω_{ZC} would be zero when Q is set such that it does not have the ambiguity condition in (7), thereby resulting in marginal inter-beam interference. When the ZC-BSP is used for beam search, the tolerance level (probability not to have a detection error) increases in asynchronous environments (where STO and CFO exist) as Q increases. However, the number of available BIDs decreases as Q increases.

In (2), Υ_{ZC} represents the inter-cell interference caused by cross-correlation when the received beam has a different CID ($c \neq \bar{c}$) regardless of its BID. The terms inside the summation in Υ_{ZC} can be derived using the Gauss sum [31], which is given in (9), as shown at the of bottom of the page. Here, $\langle\rangle$ and $\bar{Q}$ denote the Jacobi symbol [31] and reference cyclic shift spacing constant. From (9), it evident that the amplitude of (9) in Υ_{ZC} is bounded by $\sqrt{N_z}$. It should be noted that the ZC sequence has a constant envelop. In addition, most of the channel gains and beamforming gains in Υ_{ZC} are marginal because most of the Tx beams from the adjacent BSs and the Rx beam in the MS are not aligned in this case. Thus, the inter-cell interference would be marginal when the ZC-BSP is used. Finally, Ψ_{ZC} represents the noise term correlated with the reference preamble. Therefore, the horizontal BID $b_j^{BS,H}$, vertical BID $b_j^{BS,V}$, CID, and STO can be detected by determining the parameter values that yield the maximum correlation peak in (2), provided the value of Q in the ZC-BSP is set such that it does not have the ambiguity condition in (7).

IV. LFM- BASED 3D BEAMFORMING TECHNIQUE

LFM waveforms have been widely used for surveillance applications such as radar and sonar because of their robustness to the Doppler shift [32]. In radar and sonar systems, the transmitted signal is correlated with the received echo signal to estimate parameters such as range, angle, and velocity. In these systems, the information of the transmitter identity need not be carried in the transmitted signal. However, in the proposed 3D beamforming technique for mmWave cellular systems, many different preambles need to be generated to ensure that the MS can distinguish the preambles transmitted from different BSs and different beams. In the proposed LFM-based BSP (LFM-BSP), the CID and the horizontal and vertical BIDs are mapped to its frequency shift and frequency sweeping parameters, respectively. The LFM-BSP is defined as:

$$x_{LFM}^{c,b_j}(t) = e^{j\pi\left(2f_c t + \frac{\beta_{b_j}}{T_{LFM}} t^2\right)}, \quad 0 \le t \le T_{LFM} \tag{10}$$

where

$$\begin{gathered} -BW \le \beta_{b_j} \le BW \\ \frac{-BW + \left|\beta_{b_j}^{\max}\right|}{2} \le f_c \le \frac{BW - \left|\beta_{b_j}^{\max}\right|}{2} \end{gathered} \tag{11}$$

Here, β_{b_j},f_c, and T_{LFM} denote the frequency sweeping parameter, frequency shifting parameter, and symbol duration of the LFM waveform, respectively. Furthermore, $\beta_{b_j}^{\max}$ and BW denote the maximum value of frequency sweeping parameter and the available bandwidth, respectively. As the Tx beams are simultaneously transmitted in the proposed beamforming technique, the BIDs b_j are distinguished by β_{b_j} in the LFM-BSP. For notational convenience, the BID β_{b_j} is used instead of $\beta_{b_j}^{BS,H}$ for the horizontal BID and $\beta_{b_j}^{BS,V}$ for the

$$\begin{aligned} &\sum_{c=0,c\neq\bar{c}}^{N_c-1}\sum_{b_j=0}^{N_B^{BS}-1}\sum_{n=0}^{N_Z-1} x_{ZC}^{c,b_j}(n-\delta_i^c)e^{\frac{j2\pi n\varepsilon_i^c}{N_z}}\left(x_{ZC}^{\bar{c},\bar{b}}(n-m)\right)^* \\ &= \sum_{b=0}^{N_z-1} e^{\frac{j\pi r^c\left(n-\delta_i^c+Qb_j\right)\left(n-\delta_i^c+Qb_j+1\right)}{N_z}} e^{\frac{j2\pi n\varepsilon_i^c}{N_z}}\left(e^{\frac{j\pi r^{\bar{c}}\left(n-m+\bar{Q}\bar{b}\right)\left(n-m+\bar{Q}\bar{b}+1\right)}{N_z}}\right)^* \\ &= x_{ZC}^{c,b_j}(0)\left[x_{ZC}^{\bar{c},\bar{b}}(0)\right]^* \cdot e^{\frac{j\pi}{N_z}r^c\left(\left(\delta_i^c\right)^2-2Qb_j\delta_i^c-\delta_i^c\right)} \cdot e^{-\frac{j\pi}{N_z}r^{\bar{c}}\left(m^2-2Q\bar{b}m-m\right)} e^{\frac{-j\pi\varsigma}{N_z}} \cdot \rho \end{aligned} \tag{9}$$

where

$$\varsigma = \left(r^c Qb_j - r^{\bar{c}}\bar{Q}\bar{b} - r^{\bar{c}}\delta_i^c + r^{\bar{c}}m + \varepsilon_i{}^c\right)\left(\left(r^c Qb_j - r^{\bar{c}}\bar{Q}\bar{b} - r^{\bar{c}}\delta_i^c + r^{\bar{c}}m + \varepsilon_i{}^c\right)\left(r^c - r^{\bar{c}}\right)^{-1} + 1\right)$$

$$\rho = \sqrt{N_z}\cdot\begin{cases} \xi\dfrac{1-j^N}{1-j}, & r^c > r^{\bar{c}}, \\ \xi\dfrac{1+j^N}{1+j}, & r^c < r^{\bar{c}}, \end{cases} \qquad \xi = \left\langle\frac{\alpha\left|r_{c\bar{c}}\right|}{N_Z}\right\rangle e^{-j\frac{2\pi r_{c\bar{c}}\alpha\gamma^2}{N_Z}}$$

$$\gcd(r^c, N_z) = 1, \quad \gcd(r^{\bar{c}}, N_z) = 1, \ \gcd(r_{c\bar{c}}, N_z) = 1, \ \alpha = (N_z+1)/2, \ \gamma = (N_z-1)/2, \ r_{c\bar{c}} = r^c - r^{\bar{c}}$$

vertical BID. This is, because the horizontal and vertical beams are transmitted at different time slots in the proposed 3D beamforming. The CID is mapped to the frequency shift parameter (f_c) of the LFM waveform. The correlation property of an LFM-BSP in a multi-cell and multi-beam environment can be analyzed as in (12), as shown at the bottom of the page. Here, $y_i(t)$ is the received signal on the *ith* beam of an MS in the continuous-time domain.

$$\begin{aligned} r_{LFM,i}^{c,b_j}(\tau) &= \int_{t=-\infty}^{\infty} y_i(t)\left(x_{LFM}^{\bar{c},\bar{b}}(t-\tau)\right)^* dt \\ &= \sum_{c=0}^{N_c-1}\sum_{b=0}^{N_B^{BS}}\int_{t=-\infty}^{\infty} g_{TX}^{c,b_j} g_{RX,i} h_i^{c,b_j} x_{LFM}^{c,b_j}(t-\delta_i^{(c,b_j)}) e^{j2\pi\varepsilon_i^{(c,b_j)}n}\left(x_{LFM}^{\bar{c},\bar{b}}(t-\tau)\right)^* dt \\ &= \Gamma_{LFM} + \Omega_{LFM} + \Upsilon_{LFM} + \Psi_{LFM} \end{aligned} \tag{12}$$

where

$$\Gamma_{LFM}(\tau) = g_{TX}^{\bar{c},\bar{b}} g_{RX,i} \int_{t=-\infty}^{\infty} h_i^{\bar{c},\bar{b}} x_{LFM}^{\bar{c},\bar{b}}(t-\delta_i^{\bar{c}}) e^{j2\pi\varepsilon_i^{\bar{c}}t}\left(x_{LFM}^{\bar{c},\bar{b}}(t-\tau)\right)^* dt$$

$$\Omega_{LFM}(\tau) = \sum_{b=0,b_j\neq\bar{b}}^{N_B^{BS}-1} g_{TX}^{\bar{c},b_j} g_{RX,i} \int_{t=-\infty}^{\infty} h_i^{\bar{c},b_j} x_{LFM}^{\bar{c},b_j}(t-\delta_i^{\bar{c}}) e^{j2\pi\varepsilon_i^{\bar{c}}t}\left(x_{LFM}^{\bar{c},\bar{b}}(t-\tau)\right)^* dt$$

$$\Upsilon_{LFM}(\tau) = \sum_{c=0,c\neq\bar{c}}^{N_c-1}\sum_{b_j=0,b\neq\bar{b}}^{N_B^{BS}-1} g_{TX}^{c,b_j} g_{RX,i} \int_{t=-\infty}^{\infty} h_i^{c,b_j} x_{LFM}^{c,b_j}(t-\delta_i^{c}) e^{j2\pi\varepsilon_i^{c}t}\left(x_{LFM}^{\bar{c},\bar{b}}(t-\tau)\right)^* dt$$

$$\Psi_{LFM}(\tau) = g_{RX,i} \int_{t=-\infty}^{\infty} w_i(t)\left(x_{LFM}^{\bar{c},\bar{b}}(t-\tau)\right)^* e^{j2\pi\varepsilon_i^{c}t} dt$$

$$\begin{aligned} &\int_{-\infty}^{\infty} x_{LFM}^{\bar{c},\bar{b}}\left(t-\delta_i^{\bar{c}}\right)\left(x_{LFM}^{\bar{c},\bar{b}}(t-\tau)\right)^* e^{j2\pi\varepsilon_i^{\bar{c}}t} dt \\ &= \int_{-\infty}^{\infty} e^{j\pi\left(2f_{\bar{c}}(t-\delta_i^{\bar{c}})+\frac{\beta_{\bar{b}}}{T_{LFM}}(t-\delta_i^{\bar{c}})^2\right)} e^{-j\pi\left(2f_{\bar{c}}(t-\tau)+\frac{\beta_{\bar{b}}}{T_{LFM}}(t-\tau)^2\right)} e^{j2\pi\varepsilon_i^{\bar{c}}t} dt \\ &= T_{LFM}\xi_{LFM}(\tau) e^{j\pi\left(2f_{\bar{c}}\tau-2f_{\bar{c}}\delta_i^{\bar{c}}+\frac{\beta_{\bar{b}}}{T_{LFM}}\delta_i^{\bar{c}}-\beta_{\bar{b}}\delta_i^{\bar{c}}\tau+\varepsilon_i^{\bar{c}}\tau\right)} \sin c\left[\left(\varepsilon_i^{\bar{c}}T_{LFM}+\beta_{\bar{b}}\tau-\beta_{\bar{b}}\delta_i^{\bar{c}}\right)\xi_{LFM}(\tau)\right] \end{aligned} \tag{13}$$

$$\begin{aligned} &\int_{-\infty}^{\infty} x_{LFM}^{\bar{c},b_j}(t-\delta_i^{c}) e^{j2\pi\varepsilon_i^{c}t}\left(x_{LFM}^{\bar{c},\bar{b}}(t-\tau)\right)^* dt \\ &= e^{j\pi\left(2f_{\bar{c}}\tau-\frac{\beta_{\bar{b}}}{T_{LFM}}\tau^2-2f_{\bar{c}}\delta_i^{c}+\frac{\beta_{b_j}}{T_{LFM}}(\delta_i^{c})^2\right)} e^{-j\pi\Delta\beta T_{LFM}\left(\frac{\beta_{\bar{b}}\Delta\tau+\varepsilon_i^{c}T_{LFM}}{\Delta\beta T_{LFM}}\right)^2}\left(\frac{C^{b_j,\bar{b}}(\Delta\tau,\varepsilon_i^{c})+jsgn(\Delta\beta)S^{b_j,\bar{b}}(\Delta\tau,\varepsilon_i^{c})}{a^{b_j,\bar{b}}T_{LFM}}\right) \end{aligned} \tag{14}$$

where

$$\begin{aligned} \Delta\tau &= \tau-\delta_i^{c} \\ S^{b_j,\bar{b}}(\Delta\tau,\varepsilon_i^{c}) &= S\left(a^{b_j,\bar{b}}s_0+b^{b_j,\bar{b}}(\Delta\tau,\varepsilon_i^{c})\right)+S\left(a^{b_j,\bar{b}}s_{\Delta\tau}-b^{b_j,\bar{b}}(\Delta\tau,\varepsilon_i^{c})\right), \quad 0\le\Delta\tau<T_{LFM} \\ C^{b_j,\bar{b}}(\Delta\tau,\varepsilon_i^{c}) &= C\left(a^{b_j,\bar{b}}s_0+b^{b_j,\bar{b}}(\Delta\tau,\varepsilon_i^{c})\right)+C\left(a^{b_j,\bar{b}}s_{\Delta\tau}-b^{b_j,\bar{b}}(\Delta\tau,\varepsilon_i^{c})\right), \quad 0\le\Delta\tau<T_{LFM} \\ s_{\Delta\tau} &= \frac{T_{LFM}}{2}-|\Delta\tau|, \quad a^{b_j,\bar{b}}=\sqrt{\frac{|\Delta\beta|\pi}{T_{LFM}}}, \; b^{b_j,\bar{b}}(\Delta\tau,\varepsilon_i^{c})=\sqrt{|\Delta\beta|T_{LFM}\pi}\left(\frac{T_{LFM}+\beta_{\bar{b}}\Delta\tau}{\Delta\beta T_{LFM}}\right) \\ \Delta\beta &= \beta_{b_j}-\beta_{\bar{b}}, \quad \Delta\beta\neq 0 \end{aligned}$$

In (12), Γ_{LFM} represents the autocorrelation when the received beam is matched with the reference beam in the same cell. The terms inside the integral in Γ_{LFM} can be expressed as (13), shown at the bottom of the previous page, where $\xi_{LFM}(\tau) = (1 - |\tau|/T_{LFM})$. Here, $\beta_{\bar{b}}$ and $f_{\bar{c}}$ denote the reference frequency sweeping parameter and the reference frequency shift, respectively. From (13), it is evident that autocorrelation (amplitude) normalized by T_{LFM} becomes one when the shift index (τ) is matched with the STO ($\delta_i^{\bar{c}}$) and CFO is zero. Thereafter, it decreases following *sinc* pattern. The beamforming gain and channel gain in Γ_{LFM} will be high because the Tx and Rx beams are aligned. The STO can be estimated by identifying the peak position of the correlation value with the variation in shift index.

Term in Ω_{LFM} represents the inter-beam interference when the received beam has CID ($c = \bar{c}$) equivalent to that in the reference preamble and a different BID ($b_j = \bar{b}$). The terms inside the integral in Ω_{LFM} can be expressed using the Fresnel integral [33], which is given in (14), as shown at the bottom of the previous page. The *cosine* and *sine* Fresnel integrals are defined in (15), as shown at the bottom of the page, [33]. The correlation property in (14) will be evaluated in the simulation by using different parameter values. When the STO and CFO do not exist, the correlation value in (14) decreases as the difference ($\Delta\beta$) between frequency sweeping parameters increases, resulting in a reduction in the inter-beam interference.

In (12), Υ_{LFM} represents the inter-cell interference when the received beam has a different CID ($c \neq \bar{c}$) regardless of its BID. The terms inside the integral in Υ_{LFM} can be expressed using the Fresnel integral in (16), as shown at the bottom of the page. When $\beta_{b_j} = \beta_{\bar{b}}$, (16) is expressed as (17), shown at the bottom of the page. It is evident from (17) that peak value of the *sinc* function is obtained when the time shift, $\tau_s^{\beta_j,\bar{\beta}}$, is given by

$$\tau_s^{\beta_j,\bar{\beta}} = -\frac{T_{LFM}}{\beta_{\bar{b}}}\left(2\Delta f + \varepsilon_i^c\right) + \delta_i^c. \tag{18}$$

The time shift is affected by the difference among the frequency shift parameters, CFO, and STO. The peak value decreases as the time shift increases. To prevent false detection, the symbol duration T_{LFM} should be smaller than the value of $\tau_s^{\beta_j,\bar{\beta}}$ in (18), as follows:

$$T_{LFM} \leq \left|\tau_s^{\beta_j,\bar{\beta}}\right| \Rightarrow \left|\beta_{\bar{b}}\right| \leq \left|2\Delta f + \varepsilon_i^c - \beta_{\bar{b}}\delta_i^c\right| \tag{19}$$

Because ε_i^c is significantly smaller than Δf in practical scenarios, the range of Δf can be determined using (11) and (19)

$$C_n(t) = \int_0^t \cos\left(\frac{\pi s^2}{2}\right)ds,\ S_n(t) = \int_0^t \sin\left(\frac{\pi s^2}{2}\right)ds \tag{15}$$

$$\int_{-\infty}^{\infty} x_{LFM}^{c,b_j}(t-\delta_i^c)e^{j2\pi\varepsilon_i^c t}\left(x_{LFM}^{\bar{c},\bar{b}}(t-\tau)\right)^* dt$$
$$= e^{j\pi\left(2f_{\bar{c}}\tau - \frac{\beta_{\bar{b}}}{T_{LFM}}\tau^2 - 2f_c\delta_i^c + \frac{\beta_{b_j}}{T_{LFM}}(\delta_i^c)^2\right)} e^{-j\pi\Delta\beta T_{LFM}\left(\frac{2\Delta f T_{LFM} + \beta_{\bar{b}}\Delta\tau + \varepsilon_i^c T_{LFM}}{\Delta\beta T_{LFM}}\right)^2}\left(\frac{C^{b_j,\bar{b}}(\Delta\tau,\varepsilon_i^c) + jsgn(\Delta\beta)\,S^{b_j,\bar{b}}(\Delta\tau,\varepsilon_i^c)}{a^{b_j,\bar{b}}T_{LFM}}\right) \tag{16}$$

where

$$S_{\Delta f}^{b_j,\bar{b}}(\Delta\tau,\varepsilon_i^c) = S_{\Delta f}^{b_j,\bar{b}}\left(a^{b_j,\bar{b}}s_0 + b_{\Delta f}^{b_j,\bar{b}}(\Delta\tau,\varepsilon_i^c)\right) + S_{\Delta f}^{b_j,\bar{b}}\left(a^{b_j,\bar{b}}s_{\Delta\tau} - b_{\Delta f}^{b_j,\bar{b}}(\Delta\tau,\varepsilon_i^c)\right),\quad 0 \leq \Delta\tau < T_{LFM}$$
$$C_{\Delta f}^{b_j,\bar{b}}(\Delta\tau,\varepsilon_i^c) = C_{\Delta f}^{b_j,\bar{b}}\left(a^{b_j,\bar{b}}s_0 + b_{\Delta f}^{b_j,\bar{b}}(\Delta\tau,\varepsilon_i^c)\right) + C_{\Delta f}^{b_j,\bar{b}}\left(a^{b_j,\bar{b}}s_{\Delta\tau} - b_{\Delta f}^{b_j,\bar{b}}(\Delta\tau,\varepsilon_i^c)\right),\quad 0 \leq \Delta\tau < T_{LFM}$$
$$b_{\Delta f}^{b_j,\bar{b}}(\Delta\tau,\varepsilon) = \sqrt{|\Delta\beta|\,T_{LFM}\pi}\left(\frac{\left(\Delta f + \varepsilon_i^c\right)T_{LFM} + \beta_{\bar{b}}\Delta\tau}{\Delta\beta T_{LFM}}\right),\ \Delta f = f_c - f_{\bar{c}}$$

$$\int_{-\infty}^{\infty} x_{LFM}^{c,\bar{b}}(t-\delta_i^c)e^{j2\pi\varepsilon_i^c t}\left(x_{LFM}^{\bar{c},\bar{b}}(t-\tau)\right)^* dt$$
$$= e^{j\pi\left(2f_c\tau - 2f_c\delta_i^c - \frac{\beta_{\bar{b}}}{T_{LFM}}\tau^2 + \frac{\beta_{\bar{b}}}{T_{LFM}}\delta_i^{c2}\right)} \int_{-T_{LFM}/2+t}^{T_{LFM}/2} e^{j2\pi\left(2\Delta f + \frac{\beta_{\bar{b}}}{T_{LFM}}\tau - \frac{\beta_{\bar{b}}}{T_{LFM}}\delta_i^c + \varepsilon_i^c\right)t} dt$$
$$= T_{LFM}\xi_{LFM}(\tau)\, e^{j\pi\left(2f_{\bar{c}}\tau - 2f_c\delta_i^c + \frac{\beta_{\bar{b}}}{T_{LFM}}\delta_i^c - \beta_{\bar{b}}\delta_i^c\tau + \varepsilon_i^c\tau\right)} sinc\left[\left(2\Delta f T_{LFM} + \varepsilon_i^c T_{LFM} + \beta_{\bar{b}}\tau - \beta_{\bar{b}}\delta_i^c\right)\xi_{LFM}(\tau)\right] \tag{17}$$

as follows:

$$\alpha \leq \Delta f \leq \frac{BW - |\alpha|}{2} \tag{20}$$

where $\alpha = \beta_{\bar{b}} + \beta_{\bar{b}}\delta_i^c$. The condition in (20) is satisfied for all the values of α that are less than $BW/3$. Thus, to prevent time ambiguity (false detection), the frequency shift parameters (f_c) should be selected such that the difference (Δf) between these satisfy the condition in (20).

In the LFM-BSP, the cross-correlation level between two preambles decreases as the difference ($\Delta\beta$) in the frequency sweeping parameters increases. However, the number of feasible BIDs decreases with an increase in $\Delta\beta$. To determine the number of feasible sequences in the LFM-BSP, the upper bound of the cross-correlation in (16) can be derived as follows:

$$\chi\left(T_{LFM}, \Delta\beta\right) = 2\sqrt{\frac{C_{\max}^2 + S_{\max}^2}{\pi\,\Delta\beta T_{LFM}}}, \quad \Delta\beta > 0 \tag{21}$$

Here, $C_{\max}$ and $S_{\max}$ represent maximum values of the *cosine* and *sine* Fresnal integrals. Using (15), non-normalized values of $C_{\max}$ and $S_{\max}$ can be determined as 0.9775 and 0.8948, respectively. Based on $\chi\left(T_{LFM}, \Delta\beta\right)$, maximum number of feasible sequences is independent of f_c and ε_i^c. However, $\Delta\beta$ significantly affects the cross-correlation (interference) level; $\Delta\beta$ is inversely proportional to the cross-correlation level.

V. SIMULATION

In this section, the performance of the proposed 3D beamforming technique for mmWave cellular systems with a UPA is evaluated via computer simulation. The simple cellular system model shown in Fig. 1 is used for the simulation. Here, an MS receives signals from a serving cell and two neighboring cells. The performance is analyzed only for the beam search period (initialization stage, link failure case) using the proposed ZC-BSP and LFM-BSP. The BS and MS are assumed to have a UPA with 256(16×16) elements and a ULA with 16 elements(or UPA with 4×4 elements), respectively. The 5G NR specification is the baseline document for transmission and reception [34]. The carrier frequency, subcarrier spacing, and size of the fast Fourier transform (FFT) are set to 28 GHz, 120 kHz, and 4096, respectively. Thus, the maximum bandwidth of the LFM-BSP is set to 491.5 MHz ($4096 \times 120kHz$). This determines the maximum number of available preambles. The channel between the BS and MS is assumed to experience Rician fading, which consists of a LOS path and a non-LOS (NLOS) path. The NLOS path is generated by the spatial channel model (SCM) and composed of 20 rays with an azimuth spread of 2°. The k-factor is set to 15 dB. The simulation parameters are summarized in Table 1.

Fig. 2 shows the correlation property of the ZC-BSP. Here, the transmitted BID, serving CID, and cyclic shift spacing are set to $\bar{b} = 5$, $\bar{c} = 54$, and $Q = 5$, respectively. It is assumed that the transmitter and receiver are perfectly synchronized in time (i.e., No STO). The CFO is set to either zero or one.

TABLE 1. Simulation parameters.

Simulation Parameters	Values
Fast Fourier Transform (FFT) size	4096
Subcarrier spacing	120 kHz
Operational bandwidth	491.5 MHz
Symbol duration (T_{LFM})	8.34 μs
Channel model	Spatial Channel Model (SCM)
K-factor	15 dB
Number of antenna elements at BS	16×16 UPA
Number of 3D beams at BS	256
Number of horizontal beams at BS ($N_B^{BS,H}$)	16
Number of vertical beams at BS ($N_A^{BS,V}$)	16
Number of antenna elements at MS	16 ULA (or 4x4 UPA)
Antenna spacing	$\lambda/2$
Length of sequence	127
Set of predefined angles at BS (ϕ=azimuth angle, θ=elevation angle)	$\phi = \{-90^o -61.04^o -48.59^o -38.68^o -30^o -22.02^o -14.47^o -7.18^o\ 0^o\ 7.18^o\ 14.4\ 7^o\ 22.02^o\ 30^o\ 38.68^o\ 48.59^o\ 61.04^o\}$ $\theta = \{-90^o -61.04^o -48.59^o -38.68^o -30^o -22.02^o -14.47^o -7.18^o\ 0^o\ 7.18^o\ 14.4\ 7^o\ 22.02^o\ 30^o\ 38.68^o\ 48.59^o\ 61.04^o\}$

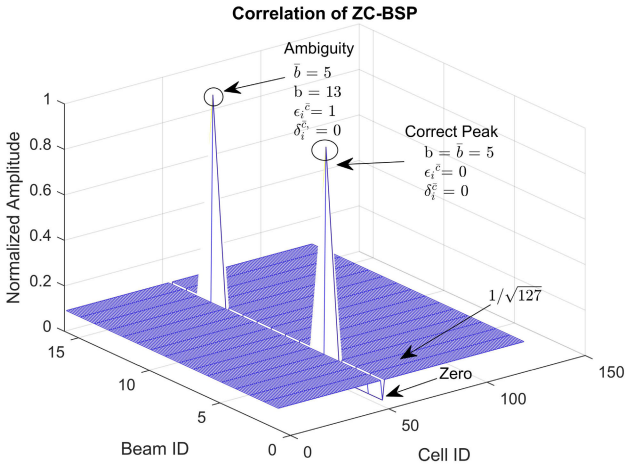

FIGURE 2. Correlation property of ZC-BSP.

It is evident that peak occurs at the correct position (CID = 54 and BID = 5) when the CFO is zero. In this case, the autocorrelation becomes one, as is evident from (3). When ($c = \bar{c}$) and ($b_j \neq \bar{b}$), the autocorrelation becomes zero as is evident from (4). However, peak occurs at an incorrect position (BID = 13) in the presence of CFO ($\varepsilon_i{}^c = 1$). This is because the ambiguity condition in (7) is satisfied. It should be noted that $Q = (17 \times 127 + 1)/54 \times (13 - 5) = 5$ when $b_j = 13$ and $\mu = 17$. Thus, the value of Q should be selected such that ambiguity condition in (7) is not satisfied when the ZC-BSP is used. It is also evident that, when the received beam has a different CID ($c \neq \bar{c}$) regardless of its BID, the amplitude of the normalized cross-correlation is given by $1/\sqrt{N_z} = 0.0887$, as is evident from (9).

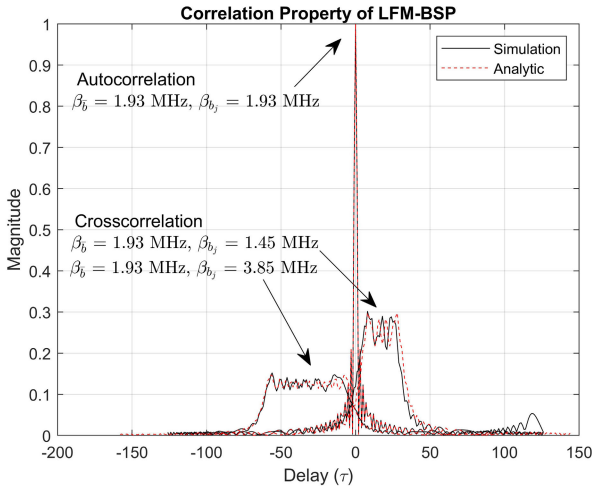

FIGURE 3. Correlation property of LFM-BSP.

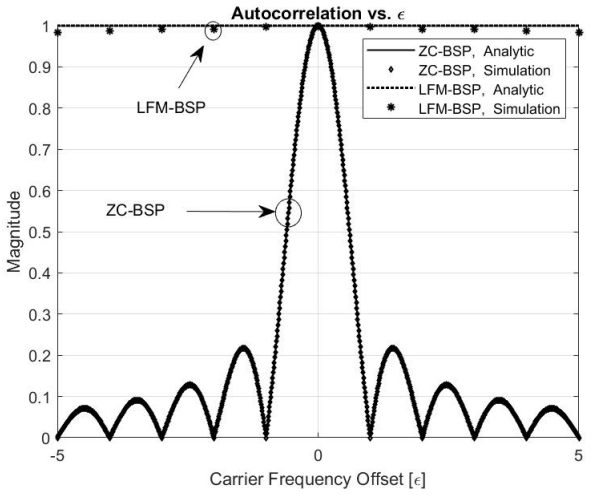

FIGURE 5. Autocorrelation properties of ZC-BSP and LFM-BSP when ε_i^c exists.

Fig. 3 shows the correlation property of the LFM-BSP when STO and CFO do not exist. Here, the value of β_{b_j} varies (1.45, 1.93, and 3.85 MHz), whereas $\beta_{\bar{b}}$ is set to 1.93 MHz. The frequency shift parameters, f_c and $f_{\bar{c}}$, are are set to zero. The autocorrelation result in this figure is obtained using (13) when β_{b_j} and $\beta_{\bar{b}}$ are equal. The cross-correlation result is obtained using (14) when β_{b_j} differs from $\beta_{\bar{b}}$. This figure indicates that the analytic results are in good agreement with the simulation results for both cases. The autocorrelation becomes one at the correct timing. Cross-correlation decreases as the difference $\Delta\beta$ between β_{b_j} and $\beta_{\bar{b}}$ increases. Thus, the inter-beam interference can be reduced if $\Delta\beta$ is sufficiently large. However, the number of feasible BIDs decreases as $\Delta\beta$ increases.

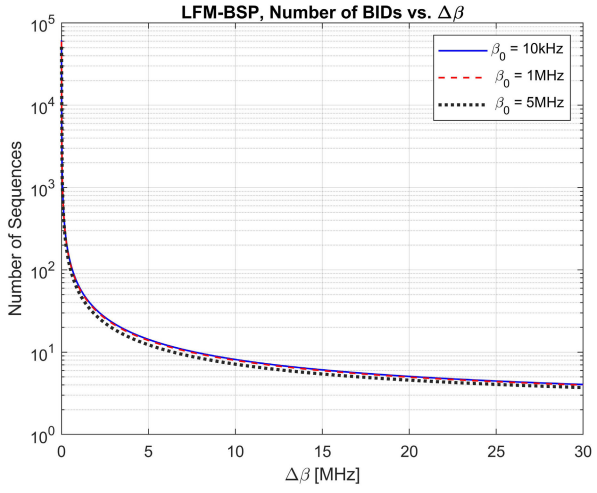

FIGURE 4. Number of LFM-BSPs vs. $\Delta\beta$.

Fig. 4 shows the number of feasible BIDs obtained using (21), when $\Delta\beta$ varies for three values of β_0. Here, β_0 denotes the starting value of β_{b_j}. From this figure, it can be verified that the number of feasible BIDs decreases with an increase in $\Delta\beta$. Thus, in the LFM-BSP, there is a trade-off between the cross-correlation level and the number of feasible sequences, during the selection of the value of $\Delta\beta$.

Fig. 5 presents comparison of autocorrelation properties of ZC-BSP and LFM-BSP when CFO exists. The analytic results of the ZC-BSP and LFM-BSP are obtained using (3) and (13), respectively. From this figure, it is evident that the analytic results are in good agreement with the simulation results. The autocorrelation of ZC-BSP decreases significantly with an increase in ε_i^c, in accordance with the *sinc* function. However, the increase in ε_i^c does not significantly affect the LFM-BSP, for a small value of CFO. This is because the LFM waveform is Doppler-insensitive. Thus, it is likely that, for high velocity applications such as V2X and UAV, the LFM-BSP can yield a higher performance owing to its robustness to ε_i^c.

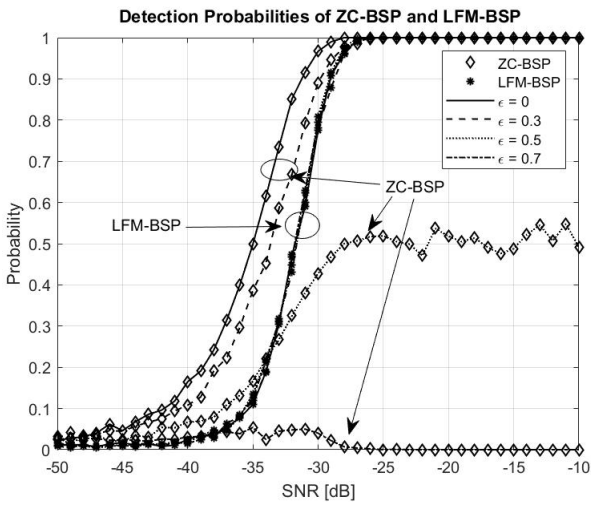

FIGURE 6. Detection probabilities of ZC-BSP and LFM-BSP.

Fig. 6 compares the detection probabilities of the ZC-BSP and LFM-BSP techniques in the presence of CFO. Here, it is assumed that the MS receives signals from a serving cell

and two neighboring cells and that the distances between the MS and three BSs are equal. This implies that the signal-to-interference ratio (SIR) is 0 dB. For both the BSPs, the sequence length is set to 127. The parameters listed in Table 1 are used for the simulation. In both the techniques, 16 beams are transmitted in parallel from the UPA. In the ZC-BSP, the 16 beams are generated with an equal root index (CID) by varying Q. The CIDs for three cells are set to 1, 2, and 3, with $\bar{c} = 2$. Q is set to seven to prevent the ambiguity condition in (7). In the LFM-BSP, $\Delta\beta$ is set to 240 kHz. f_c is set to 0, 3.84, and 7.68 MHz, with $f_{\bar{c}} = 0$. It is also assumed that the MS is located at an azimuth angle of 0° and an elevation angle of −30°. The horizontal BID 9 corresponds to an azimuth angle of 0°, and the vertical BID 5 corresponds to an elevation angle of −30°. The detection probability is obtained by correlating the received signal with a locally generated reference preamble and by determining the index that maximizes the correlation. The detection is declared "successful" when both horizontal BID and vertical BID, detected at the MS are correct. It is evident from Fig. 6 that the detection probability of the ZC-BSP decreases as ε_i^c increases. The detection probability is 0.5 when ε_i^c is 0.5, and 0 when ε_i^c is 0.7. However, the detection probability of the LFM-BSP remains unaffected by the increase in ε_i^c. When CFO is absent, the detection probability of the ZC-BSP is higher than that of the LFM-BSP. This is attributed to the good correlation property of the ZC sequence.

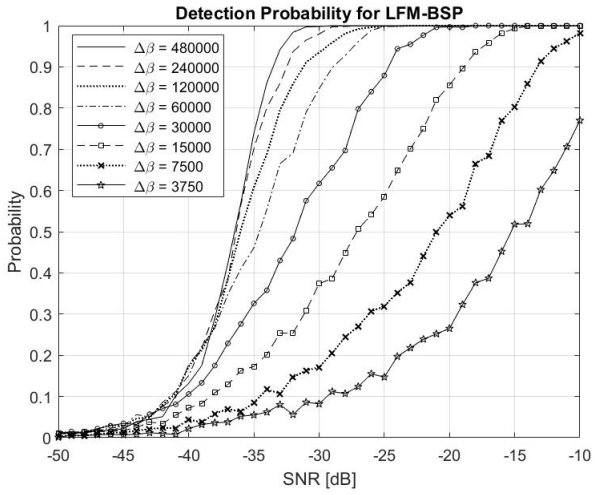

FIGURE 7. Detection probability of LFM-BSP with different $\Delta\beta$.

Fig. 7 presents the detection probability of the LFM-BSP when $\Delta\beta$ varies. The figure indicates that the detection probability increases as $\Delta\beta$ increases. However, as shown in Fig. 4 the number of feasible BIDs decreases with an increase in $\Delta\beta$. Fig. 8 depicts a comparison of the 3D beampatterns obtained using the conventional and the proposed beamforming techniques. The exhaustive search technique is used for UPA in the conventional technique, that is, individual Tx beams are transmitted from the BS until 256 beams are

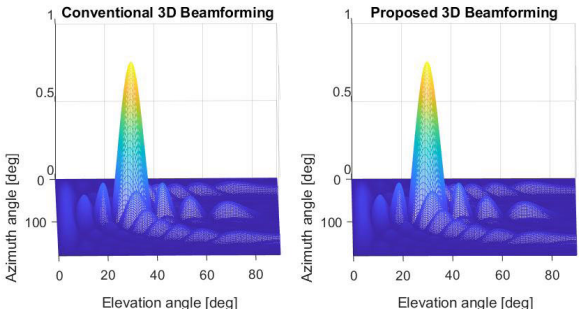

FIGURE 8. 3D beampatterns of conventional and proposed techniques.

transmitted at all the azimuth and elevation angles. The beam that produces the highest SNR at the MS is selected as the optimal Tx beam. In the proposed technique, the two-step approach is used to detect horizontal and vertical BIDs. From Fig. 8, it is evident that the 3D beampatterns obtained via both the techniques are almost identical. There is no impact on the beam pattern in the proposed 3D beamforming technique as compared to conventional 3D beamforming.

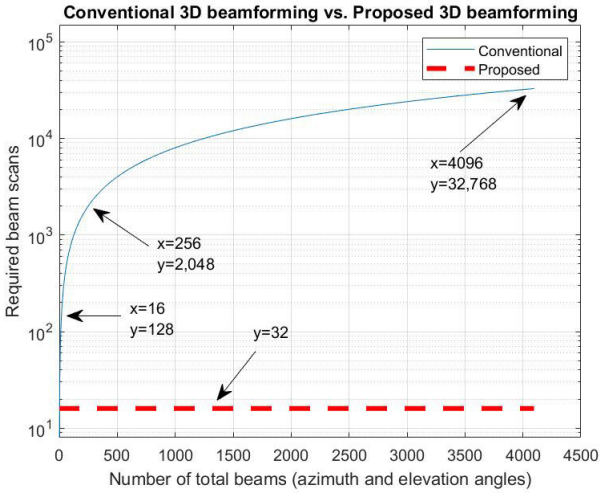

FIGURE 9. Number of beam scans required for 3D beamforming.

Fig. 9 presents a comparison of the number of beam scans required for the conventional (exhaustive search) and proposed technique when the parameters in Table 1 is used. The number of beam scans required for conventional 3D beamforming is expressed as $N_B^{BS,H} \times N_B^{BS,V} \times N_B^{MS}$. Here, N_B^{MS} denotes the number of Rx beams at the MS. If the UPA has $N_B^{BS,H}$ horizontal antenna arrays and $N_B^{BS,V}$ vertical antenna arrays, the number of beam scans required for the proposed 3D beamforming is given by $2 \times N_B^{MS}$. Thus, it is evident from Fig. 9 that the proposed technique requires a significantly lower number of beam scans than the conventional technique. It should be noted that the required number of beam scans is plotted on a log scale. For an mmWave system with 16 (4×4) Tx beams and 8 Rx beams,

the conventional technique requires 128 beam scans, whereas the proposed technique requires 32 beam scans. This difference increases as the size of the UPA increases. When the UPA has 256 (16 × 16) Tx beams and 8 Rx beams, the conventional technique requires 2,048 beam scans. When the UPA has 4,096 (64 × 64) elements, the conventional technique requires 32,768 beam scans. However, the proposed technique still requires 32 beam scans for both these cases.

VI. CONCLUSION

This paper proposes two beam search preambles (ZC-BSP and LFM-BSP) for 3D beamforming in mmWave cellular systems with UPAs, to reduce the overhead for the beam search operation. It was demonstrated via simulation that the ZC-BSP achieves a good performance (i.e., high detection probability) in the absence of CFO, owing to the good correlation property of the ZC sequence. It can also provide a large number of preambles with different CIDs and BIDs. However, its performance is significantly degraded as CFO increases. Moreover, it was demonstrated that the performance of LFM-BSP is less affected by the presence of CFO, because the LFM waveform is robust to CFO. However, its performance is degraded as the difference ($\Delta\beta$) between the frequency sweeping parameters in LFM-BSPs decreases. Thus, the performance of the LFM-BSP can be improved by increasing $\Delta\beta$. However, the number of feasible BIDs decreases with an increase in $\Delta\beta$. Thus, in the LFM-BSP, there is a trade-off between performance and the number of BIDs in selecting $\Delta\beta$. It was also shown that 3D beampatterns obtained via the conventional and proposed beamforming techniques are similar. However, the beam search time required for the proposed technique is significantly lower than that for the conventional technique; moreover, this beam search time remains constant even when the size of the UPA increases. Therefore, the ZC-BSP and LFM-BSP can be effectively used for fast 3D beamforming in fixed infrastructure networks and mobile ad hoc networks, respectively.

APPENDIX
DERIVATION OF (9)

Equation (9) can be derived in (22)–(25), as shown at the bottom of the page, where $\varsigma = (r^c Qb_j - r^{\bar{c}}\bar{Q}\bar{b} - r^{\bar{c}}\delta + r^{\bar{c}}m + \varepsilon_i{}^c)((r^c Qb_j - r^{\bar{c}}\bar{Q}\bar{b} - r^{\bar{c}}\delta_i^c + r^{\bar{c}}m + \varepsilon_i{}^c)(r^c - r^{\bar{c}})^{-1} + 1)$.

$$\sum_{n=0}^{N-1} e^{j\frac{\pi r_{c\bar{c}} n(n+1)}{N_z}}$$

$$= \sum_{n=0}^{N-1} e^{j\frac{2\pi r_{c\bar{c}}\alpha\left((n-\gamma)^2-\gamma^2+(2\gamma+1)n\right)}{N_z}} \tag{26}$$

$$= \sum_{b=0}^{N_z-1} e^{j\pi\frac{r^c\left(n-\delta_i^c+Qb_j\right)\left(n-\delta_i^c+Qb_j+1\right)+2n\varepsilon_i{}^c-r^{\bar{c}}\left(n-m+p\bar{Q}\bar{b}\right)\left(n-m+\bar{Q}\bar{b}+1\right)}{N_z}} \tag{27}$$

$$= e^{-j\frac{2\pi r_{c\bar{c}}\alpha\gamma^2}{N_z}} \sum_{n=0}^{N-1} e^{j\frac{2\pi r_{c\bar{c}}\alpha(n-\gamma)^2}{N_z}} \tag{28}$$

$$= e^{-j\frac{2\pi r_{c\bar{c}}\alpha\gamma^2}{N_z}} \begin{cases} G\left(\alpha\left|r_{c\bar{c}}\right|, N_z\right), & r^c > r^{\bar{c}} \\ G^*\left(\alpha\left|r_{c\bar{c}}\right|, N_z\right), & r^c < r^{\bar{c}} \end{cases} \tag{29}$$

Here, $\alpha = (N_z+1)/2$, $\gamma = (N_z-1)/2$ and $r_{c\bar{c}} = r^c - r^{\bar{c}}$. $G\left(\alpha\left|r_{c\bar{c}}\right|, N_z\right)$ is a Gauss Sum expression [31], given by

$$G(a, N_z) = \sum_{n=0}^{N-1} e^{j\frac{2\pi an^2}{N_z}} = \left(\frac{a}{N_z}\right)\frac{1-j^{N_Z}}{1-j}\sqrt{N_z}. \tag{30}$$

Using the above results, (22) is given by

$$x_{ZC}^{c,b_j}(0)\left[x_{ZC}^{\bar{c},\bar{b}}(0)\right]^* \cdot e^{\frac{j\pi}{N_z}r^c\left(\left(\delta_i^c\right)^2-2Qb_j\delta_i^c-\delta_i^c\right)} \cdot e^{-\frac{j\pi}{N_z}r^{\bar{c}}\left(m^2-2Q\bar{b}m-m\right)} e^{\frac{-j\pi\varsigma}{N_z}} \cdot \rho \tag{31}$$

$$\sum_{c=0,c\neq\bar{c}}^{N_c-1}\sum_{b_j=0}^{N_B^{BS}-1}\sum_{n=0}^{N_Z-1} x_{ZC}^{c,b_j}(n-\delta_i^c)e^{\frac{j2\pi n\varepsilon_i^c}{N_z}}\left(x_{ZC}^{\bar{c},\bar{b}}(n-m)\right)^* \tag{22}$$

$$= \sum_{b=0}^{N_z-1} e^{\frac{j\pi r^c\left(n-\delta_i^c+Qb_j\right)\left(n-\delta_i^c+Qb_j+1\right)}{N_z}} e^{\frac{j2\pi n\varepsilon_i^c}{N_z}}\left(e^{\frac{j\pi r^{\bar{c}}\left(n-m+\bar{Q}\bar{b}\right)\left(n-m+\bar{Q}\bar{b}+1\right)}{N_z}}\right)^*$$

$$= \sum_{b=0}^{N_z-1} e^{j\pi\frac{r^c\left(n^2+2nQb_j+n+Q^2b_j{}^2+Qb_j\right)-r^{\bar{c}}\left(n^2+2n\bar{Q}\bar{b}+n+\bar{Q}^2\bar{b}^2+\bar{Q}\bar{b}\right)+2n\varepsilon_i{}^c+r^c\left(-2n\delta_i^c+\left(\delta_i^c\right)^2-2Qb_j\delta_i^c-\delta_i^c\right)-r^{\bar{c}}\left(-2nm+m^2-2p\bar{b}m-m\right)}{N_z}} \tag{23}$$

$$= x^{c,b_j}(0)\left[x^{\bar{c},\bar{b}}(0)\right]^* e^{\frac{j\pi}{N_z}r^c\left(\left(\delta_i^c\right)^2-2Qb_j\delta_i^c-\delta_i^c\right)} e^{-j\pi\frac{r^{\bar{c}}\left(m^2-2Q\bar{b}m-m\right)}{N_z}} \sum_{k=0}^{N_z-1} e^{\frac{j\pi}{N_z}\left(r^c-r^{\bar{c}}\right)n(n+1)+2n\left(r^cQb_j-r^{\bar{c}}\bar{p}\bar{b}-r^{\bar{c}}\delta_i^c+r^{\bar{c}}m+\varepsilon_i{}^c\right)} \tag{24}$$

$$= x^{c,b_j}(0)\left[x^{\bar{c},\bar{b}}(0)\right]^* e^{\frac{j\pi}{N_z}r^c\left(\left(\delta_i^c\right)^2-2Qb_j\delta_i^c-\delta_i^c\right)} e^{-\frac{j\pi}{N_z}r^{\bar{c}}\left(m^2-2Q\bar{b}m-m\right)} e^{\frac{-j\pi}{N_z}\varsigma} \sum_{n=0}^{N_z-1} e^{\frac{j\pi}{N_z}\left(r^c-r^{\bar{c}}\right)n(n+1)} \tag{25}$$

where

$$\rho = \sqrt{N_z} \cdot \begin{cases} \xi \dfrac{1-j^N}{1-j}, & r^c > r^{\bar{c}} \\ \xi \dfrac{1+j^N}{1+j}, & r^c < r^{\bar{c}} \end{cases}$$

and $\xi = \left\langle \frac{\alpha |r_{c\bar{c}}|}{N_Z} \right\rangle e^{-j\frac{2\pi r_{c\bar{c}} \alpha \gamma^2}{N_Z}}$.

REFERENCES

[1] T. S. Rappaport, S. Sun, R. Mayzus, H. Zhao, Y. Azar, K. Wang, G. N. Wong, J. K. Schulz, M. Samimi, and F. Gutierrez, "Millimeter wave mobile communications for 5G cellular: It will work!" *IEEE Access*, vol. 1, pp. 335–349, 2013.

[2] X. Wang, L. Kong, F. Kong, F. Qiu, M. Xia, S. Arnon, and G. Chen, "Millimeter wave communication: A comprehensive survey," *IEEE Commun. Surveys Tuts.*, vol. 20, no. 3, pp. 1616–1653, 3rd Quart., 2018.

[3] T. S. Rappaport, Y. Xing, G. R. MacCartney, A. F. Molisch, E. Mellios, and J. Zhang, "Overview of millimeter wave communications for fifth-generation (5G) wireless networks—With a focus on propagation models," *IEEE Trans. Antennas Propag.*, vol. 65, no. 12, pp. 6213–6230, Dec. 2017.

[4] S. M. Razavizadeh, M. Ahn, and I. Lee, "Three-dimensional beamforming: A new enabling technology for 5G wireless networks," *IEEE Signal Process. Mag.*, vol. 31, no. 6, pp. 94–101, Nov. 2014.

[5] H. Halbauer, S. Saur, J. Koppenborg, and C. Hoek, "3D beamforming: Performance improvement for cellular networks," *Bell Labs Tech. J.*, vol. 18, no. 2, pp. 37–56, Sep. 2013.

[6] F. J. Martin-Vega, M. C. Aguayo-Torres, G. Gomez, J. T. Entrambasaguas, and T. Q. Duong, "Key technologies, modeling approaches, and challenges for millimeter-wave vehicular communications," *IEEE Commun. Mag.*, vol. 56, no. 10, pp. 28–35, Oct. 2018.

[7] C. Zhang, W. Zhang, W. Wang, L. Yang, and W. Zhang, "Research challenges and opportunities of UAV millimeter-wave communications," *IEEE Wireless Commun.*, vol. 26, no. 1, pp. 58–62, Feb. 2019.

[8] J. Choi, V. Va, N. Gonzalez-Prelcic, R. Daniels, C. R. Bhat, and R. W. Heath, Jr., "Millimeter-wave vehicular communication to support massive automotive sensing," *IEEE Commun. Mag.*, vol. 54, no. 12, pp. 160–167, Dec. 2016.

[9] W. Zhang, X. Zhou, L. Yang, Z. Zhang, B. Y. Zhao, and H. Zheng, "3D beamforming for wireless data centers," in *Proc. 10th ACM Workshop Hot Topics Netw. (HotNets-X)*. New York, NY, USA: Association for Computing Machinery, 2011, pp. 1–6, doi: 10.1145/2070562.2070566.

[10] X. Zhou, Z. Zhang, Y. Zhu, Y. Li, S. Kumar, A. Vahdat, B. Y. Zhao, and H. Zheng, "Mirror on the ceiling: Flexible wireless links for data centers," in *Proc. ACM SIGCOMM Conf. Appl., Technol., Archit., Protocols Comput. Commun. (SIGCOMM)*. New York, NY, USA: Association for Computing Machinery, 2012, p. 443–454, doi: 10.1145/2342356.2342440.

[11] E. Dahlman, S. Parkvall, and J. Sköld, *5G NR: The Next Generation Wireless Access Technology*. New York, NY, USA: Academic, 2018.

[12] *5G; NR; Physical Layer Procedures for Control*, document 3GPP TS 38.213 ETSI Ts 138 213 V15.2.0 (2018-07), 2018, vol. 15, p. 100. [Online]. Available: https://www.etsi.org

[13] S. Kutty and D. Sen, "Beamforming for millimeter wave communications: An inclusive survey," *IEEE Commun. Surveys Tuts.*, vol. 18, no. 2, pp. 949–973, 2nd Quart., 2016.

[14] W. Zhang, Y. Wang, F. Peng, and Y. Yuan, "Interference coordination with vertical beamforming in 3D MIMO-OFDMA networks," *IEEE Commun. Lett.*, vol. 18, no. 1, pp. 34–37, Jan. 2014.

[15] Q. Yuan, Y. Hu, C. Wang, and Y. Li, "Joint 3D beamforming and trajectory design for UAV-enabled mobile relaying system," *IEEE Access*, vol. 7, pp. 26488–26496, 2019.

[16] Y.-S. Cheng and C.-H. Chen, "A novel 3D beamforming scheme for LTE-advanced system," in *Proc. 16th Asia–Pacific Netw. Oper. Manage. Symp.*, Sep. 2014, pp. 1–6.

[17] M. Baianifar, S. M. Razavizadeh, S. Khavari-Moghaddam, and T. Svensson, "Effect of users height distribution on the coverage of mmWave cellular networks with 3D beamforming," *IEEE Access*, vol. 7, pp. 68091–68105, 2019.

[18] X. Li, C. Li, S. Jin, and X. Gao, "Interference coordination for 3-D beamforming-based HetNet exploiting statistical channel-state information," *IEEE Trans. Wireless Commun.*, vol. 17, no. 10, pp. 6887–6900, Oct. 2018.

[19] J. Niu, G. Y. Li, Y. Li, D. Fang, and X. Li, "Joint 3D beamforming and resource allocation for small cell wireless backhaul in HetNets," *IEEE Commun. Lett.*, vol. 21, no. 10, pp. 2286–2289, Oct. 2017.

[20] S. Mohammad Razavizadeh and T. Svensson, "3D beamforming in reconfigurable intelligent surfaces-assisted wireless communication networks," 2020, *arXiv:2001.06653*. [Online]. Available: http://arxiv.org/abs/2001.06653

[21] H. Lee, W. Ryu, W. Sung, and J. Park, "Beamforming for rotated 3D multipanel array structures for 5G NR MIMO transmission," *Int. J. Antennas Propag.*, vol. 2019, Jul. 2019, Art. no. 2830792.

[22] J. Kim and A. F. Molisch, "Fast millimeter-wave beam training with receive beamforming," *J. Commun. Netw.*, vol. 16, no. 5, pp. 512–522, Oct. 2014.

[23] E. Chen and M. Tao, "ADMM-based fast algorithm for multi-group multicast beamforming in large-scale wireless systems," *IEEE Trans. Commun.*, vol. 65, no. 6, pp. 2685–2698, Jun. 2017.

[24] Y. Fan, Y. Zhou, D. He, and W. Xia, "Fast transmit beamforming with distributed antennas," *IEEE Antennas Wireless Propag. Lett.*, vol. 16, pp. 121–124, 2017.

[25] H. Soleimani, R. Parada, S. Tomasin, and M. Zorzi, "Fast initial access for mmWave 5G systems with hybrid beamforming using online statistics learning," *IEEE Commun. Mag.*, vol. 57, no. 9, pp. 132–137, Sep. 2019.

[26] C. Jeong, J. Park, and H. Yu, "Random access in millimeter-wave beamforming cellular networks: Issues and approaches," *IEEE Commun. Mag.*, vol. 53, no. 1, pp. 180–185, Jan. 2015.

[27] M. Giordani, M. Mezzavilla, and M. Zorzi, "Initial access in 5G mmWave cellular networks," *IEEE Commun. Mag.*, vol. 54, no. 11, pp. 40–47, Nov. 2016.

[28] D. Chu, "Polyphase codes with good periodic correlation properties (corresp.)," *IEEE Trans. Inf. Theory*, vol. IT-18, no. 4, pp. 531–532, Jul. 1972.

[29] R. Frank, "Comments on 'polyphase codes with good periodic correlation properties' by Chu, David C." *IEEE Trans. Inf. Theory*, vol. IT-19, no. 2, p. 244, Mar. 1973.

[30] S. Sesia, I. Toufik, and M. Baker, *LTE—The UMTS Long Term Evolution: From Theory to Practice*. Hoboken, NJ, USA: Wiley, 2011.

[31] B. C. Berndt, R. J. Evans, and K. S. Williams, *Gauss and Jacobi Sums*. Hoboken, NJ, USA: Wiley, 1998.

[32] M. A. Richards, *Fundamentals of Radar Signal Processing*. New York, NY, USA: McGraw-Hill, 2005.

[33] I. S. Gradshteyn and I. M. Ryzhik, *Table of Integrals, Series, and Products*. New York, NY, USA: Academic, 2014.

[34] *5G; Study on Channel Model for Frequencies From 0.5 to 100 GHz*, document (3GPP TR 38.901 version 14.0.0 Release 14), TSGR, 3GPP, 2017. [Online]. Available: http://www.etsi.org/standards-search

QASIM SULTAN was born in Pakistan in 1994. He received the B.S. degree in electrical and telecommunications engineering from COMSATS University, Islamabad, Pakistan, in 2017, and the M.S. degree in electrical and electronics engineering from Chung-Ang University, Seoul, South Korea, in 2019, where he is currently pursuing the Ph.D. degree in electrical and electronics engineering.

Since 2017, he has been a Research Assistant with the Mobile Communications Laboratory, Chung-Ang University. His research interests include wireless communication systems and digital signal processing. He was a recipient of the Chung-Ang University Young Scientist Scholarship (CAYSS).

MOHAMMED SAQUIB KHAN (Graduate Student Member, IEEE) was born in Mumbai, Maharashtra, India, in 1994. He received the B.E. degree in electronics and telecommunication engineering from Mumbai University, Mumbai, India, in 2015, and the M.S. degree in electrical and electronics engineering from Chung-Ang University, Seoul, South Korea, in 2017, where he is currently pursuing the Ph.D. degree in electrical and electronics engineering.

Since 2015, he has been a Research Assistant with the Mobile Communications Laboratory, Chung-Ang University. He has authored more than 15 international articles and conference proceedings. His research interests include wireless communication systems and digital signal processing.

YONG SOO CHO (Senior Member, IEEE) was born in South Korea. He received the B.S. degree in electronics engineering from Chung-Ang University, Seoul, South Korea, in 1984, the M.S. degree in electronics engineering from Yonsei University, Seoul, in 1987, and the Ph.D. degree in electrical and computer engineering from The University of Texas at Austin, Austin, TX, USA, in 1991.

In 1984, he was a Research Engineer at Goldstar Electrical Company, Osan, South Korea. In 2001, he was a Visiting Research Fellow with the Electronics and Telecommunications Research Institute. Since 1992, he has been a Professor with the School of Electrical and Electronics Engineering, Chung-Ang University. He has authored 12 books and more than 400 conference and articles and holds more than 120 patents. His research interests include mobile communication and digital signal processing, especially for MIMO OFDM and 5G.

Dr. Cho served as the President of the Korean Institute of Communications and Information Sciences, in 2016, and was a recipient of the Dr. Irwin Jacobs Award, in 2013.